11724 *Biochemistry* **2009,** *48,* 11724–11736
DOI: 10.1021/bi900853v

BIOCHEMISTRY
including biophysical chemistry & molecular biology
Article

Physical Instability of a Therapeutic Fc Fusion Protein: Domain Contributions to Conformational and Colloidal Stability[†]

Jonas L. Fast,*[,‡,∥] Amanda A. Cordes,[‡] John F. Carpenter,[§] and Theodore W. Randolph*[,‡]

[‡]*Department of Chemical and Biological Engineering, Center for Pharmaceutical Biotechnology, University of Colorado, Boulder, Colorado 80309, and* [§]*Department of Pharmaceutical Sciences, Center for Pharmaceutical Biotechnology, University of Colorado Denver Anschutz Medical Campus, Aurora, Colorado 80045,* [∥]*Present address: Formulation R&D Biologics, Pharmaceutical and Analytical R&D, F. Hoffmann-La Roche AG, CH-4070 Basel, Switzerland.*

Received May 20, 2009; Revised Manuscript Received November 6, 2009

ABSTRACT: Protein therapeutics made up of artificially combined proteins or protein domains, so-called fusion proteins, are a novel and growing class of biopharmaceuticals. We have studied abatacept (Orencia), a fusion protein that is constructed of a modified IgG Fc domain and the soluble part of the T-cell receptor CTLA-4. In accelerated degradation studies conducted at 40 °C, a pH shift from 7.5 to 6.0 yields significantly faster aggregation kinetics, as measured by size-exclusion chromatography. To understand how the fusion domains and their interactions contribute to this result, we considered aggregation in light of the modified Lumry−Eyring reaction pathway. Protein conformational stabilities against chaotropes and temperature were measured. The structural consequences of these perturbations were observed by a variety of experimental techniques, including differential scanning calorimetry, circular dichroism, and intrinsic fluorescence. Abatacept's colloidal stability was studied by measuring zeta potentials and osmotic second virial coefficients, as well as by modeling electrostatic potentials on the protein's surface. The domains of abatacept exhibit different conformational stabilities that are highly pH dependent, whereas abatacept was weakly colloidally unstable at pH 6 or 7.5. These results are ascribed to conformational instability of the CTLA-4 and C_H2 domains, which unfold to form a molten globule-like structure that is aggregation-prone. We suggest the instability against aggregation is determined by the least stable domains.

Protein aggregation is currently a topic of widespread interest, both because of its implication in a number of human disease states (more than 50 diseases are associated with protein misfolding/aggregation, including Alzheimers', Parkinson's, and Huntington's diseases (*1*)) and because of the challenges that it presents to the biotherapeutic industry (*2*). Aggregates within therapeutic protein formulations are a safety concern because of their potential for immunogenicity and altered efficacy in patients (*3*). Aggregation of therapeutic proteins is costly, requiring additional recovery and purification steps, reducing production yields and shortening shelf life (*4*, *5*).

Recent theoretical and experimental advances have led to a greater understanding of the mechanisms by which proteins may aggregate (*4*, *6*−*9*). Using the framework of the Lumry−Eyring model (*10*), protein aggregation has been explained as requiring an initial (often reversible) unimolecular conformational change to an aggregation-competent, partially unfolded species, which then goes on to react with other protein molecules to form an aggregate that can continue to grow (*6*).

In the Lumry−Eyring framework, the observed reaction orders depend on which of the various steps is rate-limiting. In one limiting case, a first-order dependence on protein concentration is observed if the rate of unfolding to form the aggregation-competent species is slow. Alternatively, second-order kinetics may be observed if the association step in the second part of the reaction is rate limiting. In solutions where the protein is colloidally stable (e.g., at pH values removed from the isoelectric point, p*I*), k_2 may be greatly reduced. Typically, neither conformational stability nor colloidal stability dominates, and the observed reaction order is found to be concentration dependent and variable between those expected for the limiting cases.

For proteins that are composed of multiple domains, the interpretation of conformational stability is more complicated. In such cases, unfolding is frequently a multistep process, and individual domains may have different conformational stabilities and kinetics (*11*−*13*) and, presumably, different colloidal stabilities (*14*). If a partially unfolded state is involved in the aggregation reaction, we expect that the stability of the least stable domain will dominate the conformational stability contributions to aggregation. In one case, mutations lowering only the stability of the C_H2[1] domain of a therapeutic antibody resulted in

[†]Funding was provided by NIH Grant R01 EB006006.

*To whom correspondence should be addressed: J.L.F.: e-mail, jonas.fast@roche.com; fax, (303) 492-4341; telephone, (303) 492-4776. T.W.R.: e-mail, theodore.randolph@colorado.edu; fax, (303) 492-4341; telephone, (303) 492-4776.

[1]Abbreviations: CD, circular dichroism; C_H2, constant heavy chain domain 2; C_H3, constant heavy chain domain 3; CSM, center of spectral mass; CTLA-4, cytotoxic T lymphocyte-associated molecule 4; DLS, dynamic light scattering; DSC, differential scanning calorimetry; ESMS, electrospray−mass spectroscopy; Fc, fragment crystallizable; GdnHCl, guanidine hydrochloride; HPLC, high-pressure liquid chromatography; IEF, isoelectric focusing; MALDI-MS, matrix-assisted laser desorption/ionization mass spectroscopy; MWCO, molecular weight cutoff; PAGE, polyacrylamide gel electrophoresis; PDB, Protein Data Bank; rpm, revolutions per minute; SASA, solvent-accessible surface area; SEC, size-exclusion chromatography; SV-AUC, sedimentation velocity analytical ultracentrifugation; SVC, osmotic second virial coefficient; UV, ultraviolet.

 Published on Web 11/09/2009

```
                        10        20        30        40        50        60        70        80        90        100
                        ....|....|....|....|....|....|....|....|....|....|....|....|....|....|....|....|....|....|
human IgG1 Fc region    AEPKSCDKTHTCPPCPAPELLGGPSVFLFPPKPKDTLMISRTPEVTCVVVDVSHEDPEVKFNWYVDGVEVHNAKTKPREEQYNSTYRVVSVLTVLHQDWL
Modified Fc region      Q....S.....S..S........S.....................................................................
CTLA-4 region           MHVAQPAVVLASSRGIASFVCEYASPGKATEVRVTVLRQADSQVTEVCAATYMMGNELTFLDDSICTGTSSGNQVNLTIQGLRAMDTGLYICKVELMYPP

                        110       120       130       140       150       160       170       180       190       200
                        ....|....|....|....|....|....|....|....|....|....|....|....|....|....|....|....|....|....|....|
human IgG1, CH2 & CH3  NGKEYKCKVSNKALPAPIEKTISKAKGQPREPQVYTLPPSRDELTKNQVSLTCLVKGFYPSDIAVEWESNGQPENNYKTTPPVLDSDGSFFLYSKLTVDK
Modified Fc             ..........................................................................................
CTLA-4                  PYYLGIGNGTQIYVIDPEPCPDSD

                        210       220       230
                        ....|....|....|....|....|....|...
human IgG1, CH2 & CH3  SRWQQGNVFSCSVMHEALHNHYTQKSLSLSPGK
Modified Fc             ............................
```

FIGURE 1: Amino acid sequences of the CTLA-4 and the modified Fc regions of abatacept and sequence comparasion to the Fc region of human IgG1 (starting at amino acid 125) from the PDB file 1HZH. Dots indicate identical amino acids.

increased aggregation rates (*15*). Solution conditions increasing the surface tension (e.g., adding citrate and sucrose) stabilized the C_H2 domain and lowered the aggregation rate (*16*). In another case, a fusion protein constructed from human growth hormone and human albumin had its agitation-induced aggregation rate decreased when the domain with the lower stability, the growth hormone part, was stabilized by nonionic surfactants (*17*).

Therapeutic fusion proteins are a type of multidomain protein of particular current interest as biotherapeutics (*18*). Fusion proteins are constructed by splicing two or more proteins or protein domains to obtain new nonnatural polypeptides with combined functionalities of the parent proteins. Therapeutic fusion proteins may exhibit advantages such as connecting desired but previously noncoupled functions, increasing half-life, and increasing biological activity (*18*, *19*).

In naturally occurring multidomain proteins such as antibodies, the protein structure is stabilized by both inter- and intradomain interactions (*20*−*22*). For example, complete (IgG1) antibodies often show conformational stabilities that are intermediate between those of the C_H2 and C_H3 subdomains of isolated Fc domains and close to the stability of the isolated Fab domains (*23*−*26*). In contrast, because artificial fusion proteins have not coevolved, we expect that interdomain interactions might not contribute significantly to overall conformational stability and might even serve to destabilize such a construct. Likewise, we expect that the overall colloidal stability of an artificial fusion protein might be lower than that of a naturally occurring multidomain protein such as an antibody.

To investigate the conformational and colloidal stability and the domain influence on aggregation in a fusion protein system, we have studied abatacept (Orencia; Bristol-Myers Squibb, New York), an FDA-approved therapeutic fusion protein for treatment of rheumatoid arthritis. Abatacept is a fusion protein consisting of the soluble extracellular domain of human CTLA-4 (cytotoxic T lymphocyte-associated molecule 4) receptor that is expressed by activated T cells fused to a modified version of the Fc domain of human immunoglobulin G1, IgG1 (*27*). Abatacept is a first-in-class drug for selective costimulation modulators, designed to block a key costimulatory signal (CD80/CD86) required for T cell activation (*28*).

Structurally, abatacept is a glycosylated fusion protein with a MALDI-MS molecular mass of 92300 Da, and it is a homodimer of two homologous polypeptide chains of 357 amino acids each (for amino acid sequence and structural model see Figure 1 and Figure 2, respectively). An intermolecular disulfide bond between the CTLA-4 domains of the fusion protein links the two chains. Three cysteines and one proline in the hinge region of the Fc domain are mutated to serines, thus abolishing the native

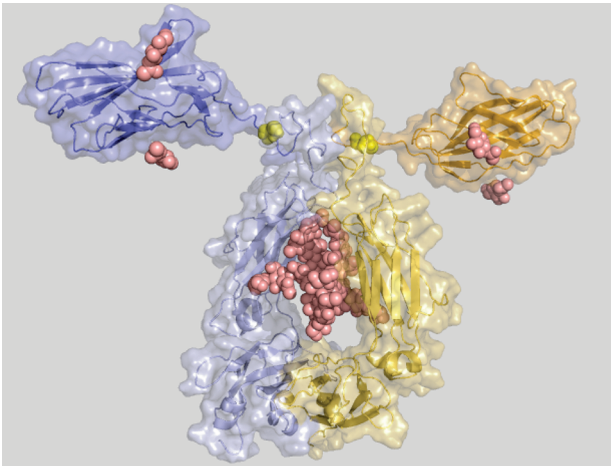

FIGURE 2: Structural model of abatacept. Blue and yellow cartoon and surface representations for each chain. Small domains (top) are the extracellular soluble domains of human CTLA-4. Large domains are the C_H2 and C_H3 domains in the modified Fc part of human IgG1. Yellow spheres are Cys120 in CTLA-4 that makes a disulfide connection between the chains. Sugar residues are represented as pink spheres. The amino acid sequence of one chain of abatacept was sent to the Robetta server (http://robetta.bakerlab.org/) for structure prediction. Robetta models were aligned in PyMOL (http://pymol.org/) with the heavy chains of IgG1 from 1HZH to build a dimer. To create the final dimer model, the CTLA-4 domain predicted by Robetta was replaced by the actual crystal structure of CTLA-4 (PDB id 1I8L) by aligning the crystal structure with each of the modeled domains in the dimer model. Graphics were made in PyMOL.

covalent Fc-chain connection as well as its complement-dependent cytotoxicity (CDC) or antibody-dependent cellular cytotoxicity (ADCC) properties (*29*). In addition, the CTLA-4 domain and the Fc domain each have four intramolecular disulfide bridges. In the dimer there are four N-linked glycosylation sites in the CTLA-4 domain and two in the Fc domain. Potentially there is an O-linked glycosylation on the P139S mutation site in the Fc domain (*29*). Heterogenous glycosylation gives a p*I* of 4.5−5.5. Abatacept has eight tryptophan residues, all exclusively located in the Fc domain, and 30 tyrosine residues distributed over both domains.

To probe the roles of abatacept's two domains in determining its overall solution stability, we conducted "accelerated degradation studies" to determine the stability of abatacept against aggregation at elevated storage temperatures (40 °C) and in various solution conditions (pH 6.0 and 7.5). We then used a variety of physical and spectroscopic techniques to elucidate the contributions of the two domains to that stability. In order to probe the conformational stability of abatacept and its domains,

chaotrope-induced and thermally induced structural perturbations were monitored using absorption and fluorescence spectroscopy, circular dichroism (CD), differential scanning calorimetry (DSC), and ANS binding. Colloidal stability was measured by static light scattering (SLS) and the zeta potential.

MATERIALS AND METHODS

All chemicals and reagents were of highest laboratory purity and obtained from Fisher Scientific (Pittsburgh, PA) and Sigma-Aldrich (St. Louis, MO) unless otherwise indicated.

Abatacept (CTLA4-Ig, Orencia; Bristol Myers Squibb, New York) was purchased (University of Colorado at Boulder Wardenburg Pharmacy) as a lyophilized powder in vials containing 250 mg of protein, 500 mg of maltose, 17.2 mg of monobasic sodium phosphate, and 14.1 mg of NaCl. CTLA-4 extracellular soluble domain (further only called CTLA-4) expressed in *Escherichia coli* was donated by Barofold Inc. (Boulder, CO).

Dialysis and Sample Preparation. One vial of lyophilized abatacept formulation was dissolved in 10 mL of USP water. Exipients were removed by extensive dialysis against Millipore water for >10 h at room temperature with at least two water changes. The protein was further dialyzed into a buffer using slide-a-lyzer dialysis cassettes (MWCO 10000 Da; Thermo-Fisher) with two to three buffer exchanges over >10 h at room temperature. Purity and no significant protein loss were confirmed by SDS−PAGE and UV absorption. Protein stock solutions at protein concentrations of typically 20−25 mg/mL were stored at 4 °C and showed no aggregation (samples contain <2% dimer fraction that does not change over time) over more than 3 months as monitored by analytical ultracentrifugation and SEC-HPLC. Samples were filtered through a 0.22 μm PVDF syringe filter (Whatman) prior to experiments.

The ionization heat of sodium phosphate buffer is small, and thus, the pH of phosphate buffer is almost constant with rising temperature. Due to this and the similarity to the therapeutic formulation, we used 10 mM mono/dibasic sodium phosphate and 25 mM NaCl, at pH 6 or 7.5. All buffers were filtered through a 0.22 μm PVDF syringe filter (Whatman) and degassed prior use.

Protein Concentration Determination. UV absorbance was measured using a Lambda 35 UV/vis spectrophotometer (Perkin-Elmer, Waltham, MA). The extinction coefficient (ε_{280}) for abatacept was calculated to be 1.0 mL mg^{-1} cm^{-1} by the ±GdnHCl method by Pace et al. (*30*), which also was cross-correlated with the amount of lyophilized protein in the vials. The extinction coefficient (ε_{280}) for *E. coli*-expressed CTLA-4 was 0.6 mL mg^{-1} cm^{-1}.

Accelerated Degradation Studies. For the reaction rate studies, a 5 mg/mL solution of abatacept in 10 mM sodium phosphate, 25 mM sodium chloride, and 0.1 g/L sodium azide, pH 6 or 7.5, was aliquoted into 100 μL samples in microcentrifuge tubes (0.6 mL; Fisher). Samples were then incubated at room temperature (ca. 22 °C) or 40 °C. Three samples per condition were removed at each time point, centrifuged for 5 min to remove insoluble aggregates, and analyzed on a Beckman Coulter System Gold 126 HPLC (Fullerton, CA) equipped with a Beckman Coulter 166 detector, a Waters 717 autosampler (Milford, MA), and a TSK-Gel 3000SWXL size-exclusion column with guard column (Tosoh Biosciences, Montgomeryville, PA). Run time was 40 min with a flow rate of 0.6 mL/min. Sample injection volumes were 40 μL, and the mobile phase was 100 mM sodium phosphate, 300 mM sodium chloride, and 0.1 g/L sodium azide, pH 7. Data were analyzed using Thermo Galactic GRAMS AI software (v.7), and the concentration of remaining monomer was calculated according to the method outlined earlier (*31*, *32*).

The initial rate of aggregation, measured at the starting protein concentration of 5 mg/mL, was calculated from triplicate measurements at five separate time points. These time points were chosen so that there was less than 10% conversion of the initial monomer to dimers and other multimers. At this limited conversion, all multimers were soluble, and the observed total peak areas (monomer/dimer/multimer for pH 6 and monomer/dimer for pH 7.5) were equal to the initial peak area for the starting monomer (within error). No lag phase was observed before aggregation began.

Deglycosylation of Abatacept. N-Linked deglycoslylation was performed with 1 unit of PNGase F/100 μg of protein in 1% *n*-octyl *p*-D-glucopyranoside (OG). Samples were incubated at 37 °C between 2 and 24 h. Deglycosylation was monitored by isoelectric focusing (IEF) PAGE, MALDI-MS, and ES-MS. After 5 h incubation with enzyme, no further changes in IEF mobility were observed.

Chaotrope-Induced Unfolding of Abatacept. Samples containing 0−6 M guanidine hydrochloride (GdnHCl) or 0−9.75 M urea were mixed from stock solutions of 17 mg/mL abatacept, buffer with 7 M GdnHCl or 10 M urea, and buffer. All stock solutions were at pH 6 or 7.5. Identical samples were mixed without protein for background measurements. Protein and background samples were incubated overnight at 4 °C before measurements. Reversibility was monitored by incubating a stock solution of 4.5 mg/mL abatacept in 8 M GdnHCl overnight at 4 °C. This stock solution was mixed with 8 M GdnHCl solution and buffer in proportions to yield samples in the range from 0.25 to 6.25 M GdnHCl. Those samples were further incubated at 4 °C overnight before fluorescence measurements at 25 °C.

Fluorescence Spectroscopy. Sample concentrations were 0.1 mg/mL abatacept in sodium phosphate buffer at pH 6 or 7.5. The protein solution was placed in a 5 mm path length square quartz cuvette thermostated at 25 °C on an Aminco Bowman Series 2 fluorescence spectrophotometer (SLM Aminco, Urbana, IL). Samples were excited at 280 or 295 nm, and emission was collected between 305 and 400 nm with excitation and emission slits of 4 nm and scan rate 50 nm/min. Background correction was performed; total fluorescence intensity and center of spectral mass (CSM) were calculated as

$$\mathrm{CSM} = \frac{\sum F_i \nu_i}{\sum F_i} \quad (1)$$

where F_i is the fluorescence intensity at wavenumber ν_i and $\sum F_i$ is the spectral integral in the spectrum range. Triplicate samples were collected, and fitting was performed as described below.

Fourth Derivative UV Absorption Spectroscopy. Fourth derivative UV absorption (4DUV) spectroscopy as a function of GdnHCl was carried out at 25 °C at pH 6 and 7.5 with samples prepared as above with a protein concentration of 0.5 mg/mL. Absorbance spectra between 260 and 305 nm were recorded in steps of 0.1 nm as a function of denaturant (averaging three scans per sample) using a Lambda 35 UV/vis spectrophotometer (Perkin-Elmer, Waltham, MA). 4DUV spectra were determined as described (*33*). Transitions between spectral forms were quantified within the 275−290 nm range, typical of Tyr effects, by cumulative difference amplitude (CDA) as reported (*34*).

ANS Fluorescence. Freshly made 8-anilino-1-naphthalenesulfonic acid (ANS) stock solutions (final concentration 100 μM) were mixed with protein and GdnHCl stock solutions to yield samples containing 0.1 mg/mL abatacept (ca. 1 μM), 100 μM ANS, and various concentrations of GdnHCl. Samples containing only ANS and GdnHCl were also prepared as background blanks for each point. Excitation wavelength was 350 nm, and the emission wavelength range was 400−600 nm with 4 nm slit widths. ANS fluorescence intensity was plotted at 480 nm as a function of GdnHCl after background spectra were subtracted from protein spectra.

Circular Dichroism. Far-UV circular dichroism (CD) spectra were obtained using a JASCO J-820 spectropolarimeter with a JASCO PTC-343 Peltier-type thermostated cell holder. Quartz cuvettes with 0.1 or 1 mm path length were used for spectra recorded between 195 and 250 nm. Near-UV CD spectra were recorded between 260 and 340 nm using a 10 × 10 mm cuvette. Abatacept and CTLA-4 concentrations were <24 and <2 μM, respectively, for far-UV CD and ~30 μM for abatacept for near-UV CD. The following settings were used: temperature, 10 °C; resolution, 1 nm; bandwidth, 1 nm; sensitivity, 20 mdeg; response time, 8 s; accumulation, 6; and scan rate, 50 nm/min. Baseline spectra were recorded with pure buffer in the cuvette and subtracted from the spectra for protein solutions. Data are reported as molar ellipticity and were determined as

$$[\theta]_\lambda = \frac{\theta_\lambda M_w}{10ncl} \quad (\text{deg cm}^2\ \text{dmol}^{-1}\ \text{residue}^{-1}) \tag{2}$$

where c is the protein concentration (mg/mL), l is the path length of the cell (cm), θ_λ is the measured ellipticity at wavelength λ (mdeg), M_w is the molecular mass of the protein (g/mol), and n is the number of residues.

Thermally Induced Unfolding of Abatacept. Fluorescence Spectroscopy. Thermally induced unfolding of abatacept was performed on a Photon Technology International (PTI) spectrofluorometer (Lawrenceville, NJ) equipped with a turreted four-position Peltier-controlled cell holder and a xenon lamp. Sample concentrations were 0.1 mg/mL in sodium phosphate buffer at pH 6 and 7.5. The protein solution was placed in a 10 mm path length triangular quartz cuvette with a Teflon cap. Tryptophan fluorescence was excited at 295 nm. Emission was collected between 305 and 400 nm with 4 nm slit widths and a scan rate of 50 nm/min. Thermally induced denaturation was followed by a scan every 2.5 or 5 °C between 10 and 90 °C. Hold time at each scan temperature was 1 min and ramping rate was 1 °C/min. After background correction, total fluorescence intensity was integrated, and center of spectral mass was calculated as above. Triplicate samples were collected, and fitting was performed as described below.

Circular Dichroism. Thermal melts were acquired for samples in phosphate buffer at pH 6 and 7.5 by monitoring the CD signal at 217 nm over the temperature range from 10 to 90 °C at intervals of 1 °C with a scanning rate of 1 °C/min; bandwidth, 2 nm; sensitivity, 20 mdeg; response time, 16 s. Blank buffer scans were subtracted from protein scans, and data were transformed to molar ellipticity as above. Fitting was performed as described below.

Differential Scanning Calorimetry. Calorimetric experiments were performed on a VP-DSC (Microcal LLC, Northampton, MA) with an active cell volume of 0.5 mL at 1.5 atm overpressure using scanning rates of 15, 30, 60, or 90 °C/min. Dialyzed and degassed samples with a protein concentration of 0.5−11 mg/mL were monitored from 5 to 115 °C in phosphate buffer. All transition midpoint temperatures are apparent as the system was not fully reversible under any experimental conditions used. Specifically, the posttransition baseline did not reach a steady baseline level, and there was no or only minor transition/excess enthalpy on repetitive runs on the same sample. Visual inspection of each sample following heat denaturation showed clear solutions for phosphate-buffered solutions. Buffer scans were subtracted from the sample scans followed by normalization for protein concentration and baseline correction using standard procedures in Origin v7.0 (Microcal LLC, Northampton, MA). Resulting apparent excess heat capacity thermograms were nonlinearly fitted to a non-two-state model with two or three transitions in Origin v7.0.

Activation Energies for Abatacept Structural Transitions. Different scanning rates (v = 15, 30, 60, and 90 °C/h) were employed to estimate the activation energy (E_a) for each thermally induced structural transition of abatacept, using the approach described by Sanchez-Ruiz (*35*), where activation energies were estimated from the slope of a plot of $\ln(v/T_m^2)$ vs $1/T_m$ using eq 3:

$$\ln\left(\frac{v}{T_m^2}\right) = \frac{AR}{E_a} - \frac{E_a}{RT_m} \tag{3}$$

where A is a preexponential factor in the Arrhenius equation, E_a is the activation energy, R is the gas constant, v is defined as the scan rate, and T_m is the midpoint transition temperature.

Data Analysis of Unfolding Curves. The CD, fluorescence, and absorbance denaturation data were analyzed using the software Kaleidagraph (Synergy Software, Reading, PA), Sigmaplot 11 (Systat Software Inc., San Jose, CA), or Origin v7.0 (Microcal LLC, Northampton, MA). Denaturation data for each transition were fitted to a two-state folding model using a nonlinear least-squares method to determine thermodynamic parameters (*36*, *37*):

$$Y_0 = \frac{(k_N[D] + b_N) + (k_U[D] + b_U)\exp\left(\frac{-\Delta G_{NU}}{RT}\right)}{1 + \exp\left(\frac{-\Delta G_{NU}}{RT}\right)} \tag{4}$$

where Y_0 is the response signal, k_N, b_N, k_U, and b_U are the intercepts and the slopes of the baselines of the native and the unfolded states (or, more specifically, the intermediate state in the case of the first transition's end state and the second transition's start state), respectively, and are assumed to be linear, ΔG_{NU} is the free energy of unfolding, R is the molar gas constant, and T is temperature. The free energy expressions for the different perturbations are outlined below:

Chaotrope-Induced Unfolding.

$$\Delta G_{NU}(D) = \Delta G_{NU}(H_2O) + m[D] \tag{5}$$

where [D] is the chaotrope concentration, $\Delta G_{NU}(H_2O)$ is the unfolding free energy in buffer without denaturant, and m is the influence of denaturant concentration on the stability and is related to the change in surface area and heat capacity change (*38*).

Thermally Induced Unfolding.

$$\Delta G_{NU}(T) = \Delta H_{NU}\left(1 - \frac{T}{T_m}\right) + \Delta C_p\left[(T - T_m) - T\ln\left(\frac{T}{T_m}\right)\right] \tag{6}$$

where T_m is the apparent transition midpoint and ΔH_{NU} is the enthalpy difference between the two states at T_m. ΔC_p is the heat capacity difference between unfolded and native protein. The T_m values are not sensitive to the value of ΔC_p.

Light Scattering. Static light scattering was used to estimate the osmotic second virial coefficient (SVC), representing overall attractive or repulsive solution-specific interactions, as a measure of the collodial stability. Samples consisted of protein concentrations ranging from 0.5 to 5 mg/mL in 10 mM sodium phosphate and 25 mM NaCl, pH 6 or 7.5, and the temperature was controlled at 24 °C. An Electro-Optics laser, model 1145AP (Hsintien City, Taiwan), and a Brookhaven Instruments goniometer and cascade photodiode detector, models BI-200SM and BI-APD (Holtsville, NY), respectively, were used to determine the excess Rayleigh ratios at a 90° angle (scattering due to protein only) to the incident 633 nm light beam. The relationship used to determine the SVC is given here and is derived from the virial expansion of the ideal osmotic pressure equation (*39*):

$$\frac{Kc}{R_{90}} = \frac{1}{M_w} + 2(\mathrm{SVC})c \tag{7}$$

where M_w is the mass-averaged molecular weight, R_{90} is the excess Rayleigh ratio at 90° (*39*), and the optical constant K is described by

$$K = \frac{4\pi^2 n_0^2 (\mathrm{d}n/\mathrm{d}c)^2}{N_A \lambda^4} \tag{8}$$

where n_0 is the refractive index of the solvent, $\mathrm{d}n/\mathrm{d}c$ is the refractive index increment, and λ is the wavelength of the incident beam. A refractive index increment of 0.185 mL/g, estimated from a weight-averaged contribution from the protein and carbohydrate portions of the monoclonal antibody, was used for all light scattering analyses (*40*).

Dynamic Light Scattering. For the dynamic light scattering a Malvern Zetasizer Nano ZS (Malvern, U.K.) was used. Protein concentration was 5 mg/mL in 10 mM sodium phosphate and 25 mM NaCl, pH 6 or 7.5. The resulting correlation functions were used to determine the diffusion coefficients from which the hydrodynamic diameters were calculated by the Stokes equation. The temperature for all light scattering measurements was controlled at 25 °C. The hydrodynamic diameter of abatacept determined by DLS (10.2 ± 0.2 nm) did not vary significantly with the solvent conditions used in this study.

Zeta Potentials. A Malvern Zetasizer Nano ZS (Malvern, U.K.) was used to measure the electrophoretic mobility of the antibody via laser Doppler velocimetry. The zeta potential is calculated from Henry's equation using the Smoluchoski approximation which is valid for ionic strengths above 1 mM (*41*):

$$\mu_e = \frac{2\varepsilon k_s \zeta}{3\eta} \tag{9}$$

where μ_e is the electrophoretic mobility, ε is the dielectric constant or permittivity of the solution, k_s is a model-based constant which from the Smoluchoski approximation is 1.5, and ζ is the zeta potential. Abatacept at 5 mg/mL in 10 mM sodium phosphate and 25 mM NaCl, pH 6 or 7.5, was used for all samples. The measurement was repeated on three samples at 25 °C, and the errors are reported as the standard deviation.

The effective charge of an equivalent sphere can be estimated via the linearized Poisson−Boltzmann equation, also referred to as the Debye−Hückel approximation, and is given by eq 10 (*42*):

$$Z = \frac{4\pi\varepsilon r_p (1 + \kappa r_p)\zeta}{e} \tag{10}$$

where Z is the effective charge, r_p is the effective sphere radius, κ is the inverse electric double layer thickness or inverse Debye length, and e is the elementary charge.

The electrostatic contribution to the SVC, also referred to as the Donnan term, can be calculated using eq 11 (*43*):

$$\mathrm{SVC}_{\mathrm{electrostatic}} = \frac{Z^2}{4M_w^2 \rho_s m_{\mathrm{ions}}} \tag{11}$$

Here $\mathrm{SVC}_{\mathrm{electrostatic}}$ is the electrostatic component of the SVC, M_w is the actual molecular weight of the protein, ρ_s is the solvent density, and m_{ions} is the molal concentration of ions.

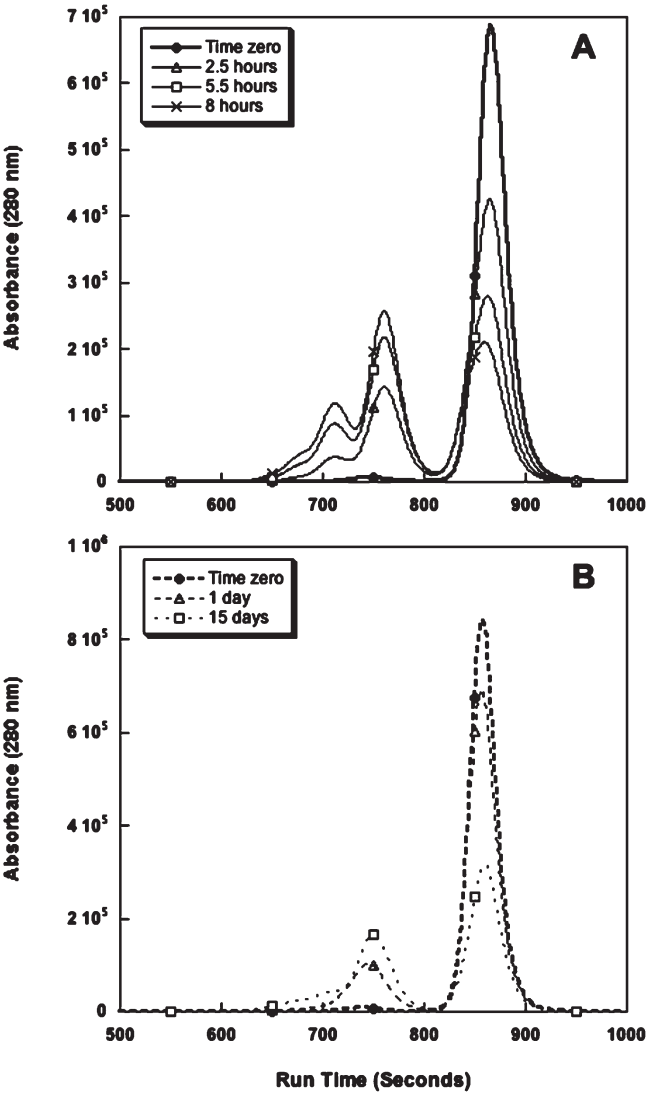

FIGURE 3: Accelerated stability studies of abatacept at 40 °C followed by SEC-HPLC at (A) pH 6 (solid) and (B) pH 7.5 (dashed). About 50% monomer loss is reached after 8 h and 15 days at pH 6 and 7.5, respectively.

RESULTS

Aggregation Reaction Rates from Accelerated Degradation Studies of Abatacept. Aggregation reaction rates were

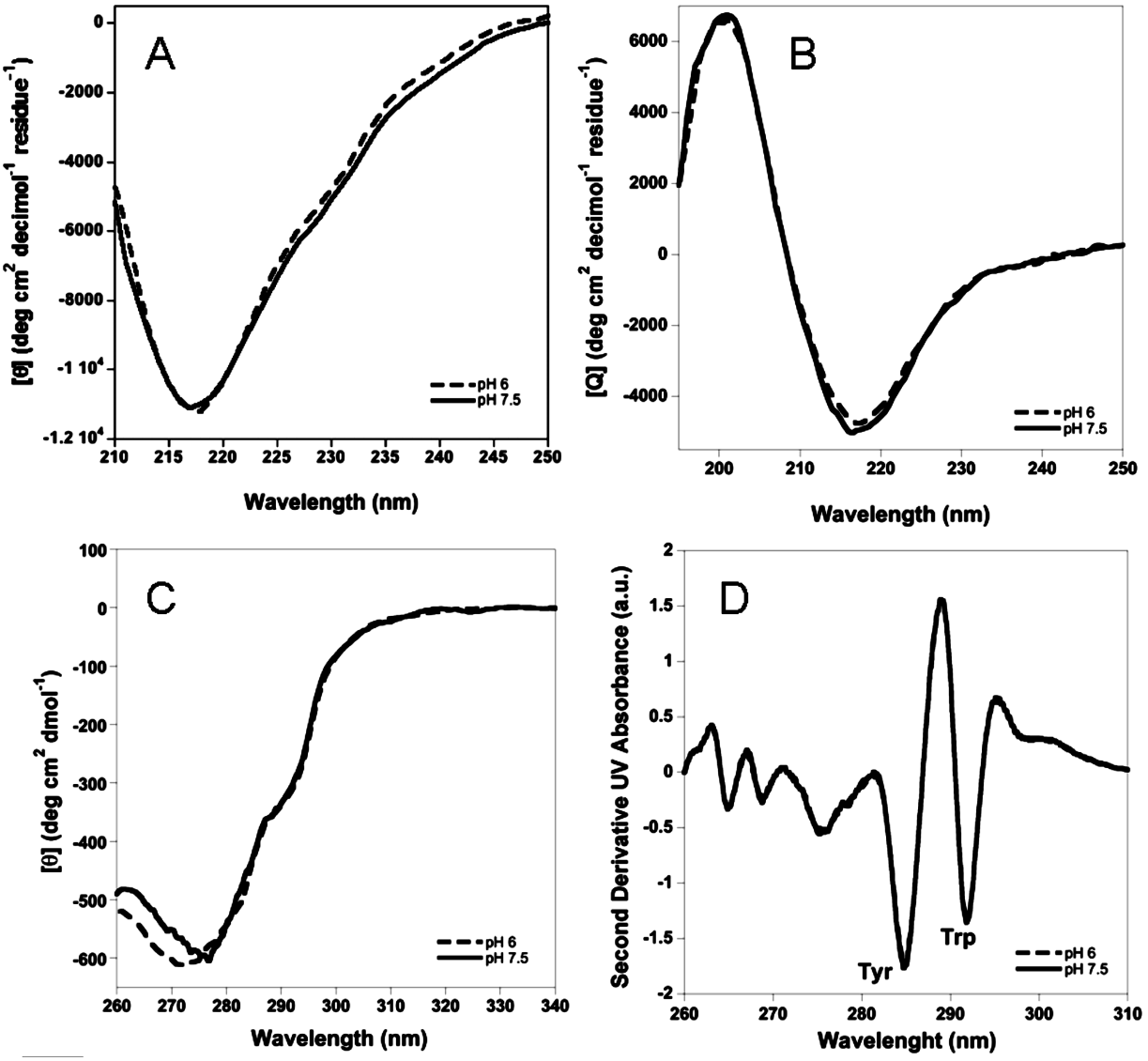

FIGURE 4: (A) Far-UV CD of abatacept. (B) Far-UV CD of CTLA-4. (C) Near-UV CD of abatacept. All at 10 °C. (D) Second derivative UV absorbance spectra overlapping at both pHs at 20 °C. Protein in 10 mM sodium phosphate buffer with 25 mM NaCl at pH 6 (dashed line) and pH 7.5 (solid line).

measured after incubation at 40 °C at either pH 6 or pH 7.5. Panels A and B of Figure 3 correspond to the 40 °C incubation experiments at pH 6 and 7.5, respectively. From these chromatograms it is apparent that the aggregation of abatacept proceeds much more rapidly at the lower pH. After only 8 h of incubation at pH 6, 40 °C, half of the monomer has associated into higher order oligomers. For pH 7.5, 15 days of incubation were needed to see the same decrease in the monomer peak. The rate of monomer loss (subsequently referred to as the aggregation rate) is 2 orders of magnitude faster at pH 6 than at pH 7.5 (800 μg/(mL h) at pH 6 versus 6 μg/(mL h) at pH 7.5). At room temperature (ca. 22 °C), less than 1% loss of monomer was seen over the course of 1 month at pH 7.5 and less than 2% of initial monomer was lost over the same period at pH 6.0 (data not shown). A fraction of dimer corresponding to less than 2% of the total protein is present after dissolving the lyophilized protein.

In studies conducted at 40 °C, the majority of higher order complexes are soluble dimers and trimers, as seen by SEC-HPLC and cross-validated with sedimentation velocity analytical ultracentrifugation (data not shown; see Supporting Information for more details). Reducing and nonreducing polyacrylamide gel electrophoresis shows that the aggregates are noncovalent (data not shown).

Reversibility of Abatacept Aggregates. The reversibility of abatacept aggregation was briefly examined. Samples were incubated at 40 °C in pH 6 buffer for 5.5 h. Half of the samples were analyzed immediately following incubation while the remaining samples were stored at 4 °C for 24 h prior to analysis. The sample stored at 4 °C prior to analysis shows an increase in the monomer peak area of ca. 18%, compared to samples analyzed immediately, as well as a decrease in the oligomeric peaks (Supporting Information Figure 1). This indicates the aggregates may be at least partially reversible.

Conformation of Abatacept and E. coli-Expressed CTLA-4 at pH 6 and 7.5. Structural features of abatacept at pH 6 and 7.5 were monitored using circular dichroism (CD), absorbance, SEC-HPLC, gels, and SV-AUC. Far-UV CD spectra at 10 °C at pH 6 and 7.5 are essentially identical and show a single minimum at 217 nm, a signature typical for β-sheet-rich proteins (Figure 4A). Near-UV CD spectra at 10 °C show differences below 280 nm, with a minimum of ca. 272 nm at pH 6 and ca. 277 nm at pH 7.5 (Figure 4C), whereas second

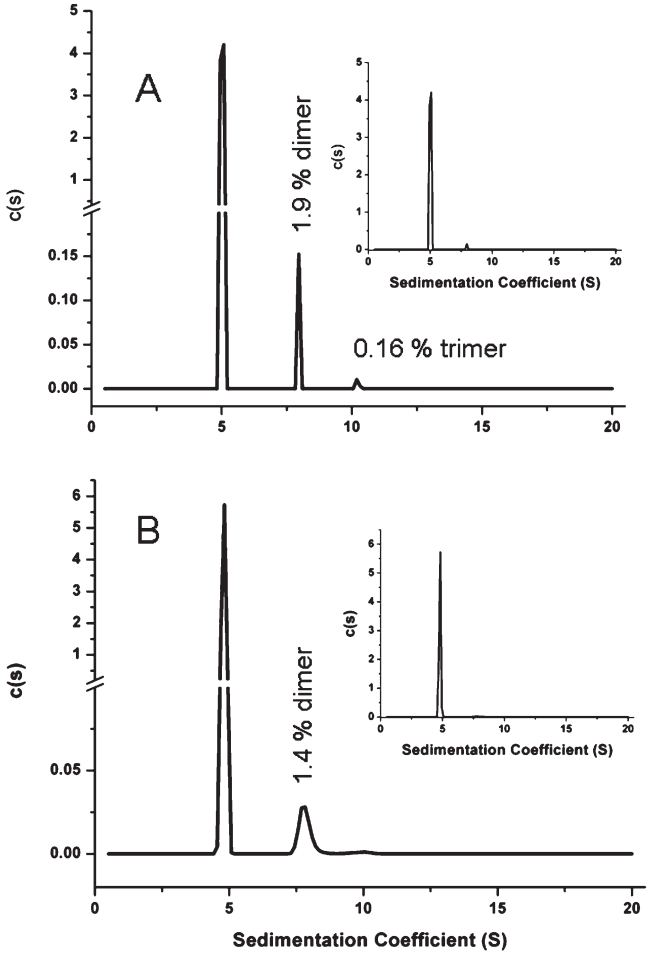

FIGURE 5: Sedimentation velocity analytical centrifugation distributions of 1.3 mg/mL abatacept in 10 mM sodium phosphate and 25 mM NaCl at pH 6 (A) and pH 7.5 (B) at 20 °C. Inserts show $c(s)$ distributions in full scale.

derivative UV absorbance spectra at 25 °C at pH 6 and 7.5 completely overlap (Figure 4D). This implies that abatacept has a very similar secondary structure at the two pH conditions tested with some differences in the environment around aromatic residues. Additionally, SEC-HPLC, SDS and native PAGE, and SV-AUC studies conducted at 4 or 20 °C at pH 6 or 7.5 show that abatacept is monomeric under the these solution conditions with $<2\%$ dimer present (Figure 5).

Using nonreducing SDS−PAGE and SV-AUC, *E. coli*-expressed CTLA-4 is shown to be $>99\%$ monomeric (data not shown). The CTLA-4 domain shows a far-UV CD spectrum similar to that of abatacept with a minimum of 217 nm and the characteristics of a β-sheet protein (Figure 4B).

Assignment of Unfolding Transitions of Abatacept. We observe two major structural transitions for abatacept upon perturbation with chaotrope or temperature (see below for more details), which we anticipate are due to unfolding of the individual Fc and CTLA-4 polypeptides that comprise the domains of the abatacept fusion protein. In order to assign these transitions, we first measured the unfolding properties of separated, individual domains. To that end, we attempted to cleave the linking region between the Fc and CTLA-4 domains of abatacept using papain (*44*) and thrombin (*45*). However, application of papain resulted in additional, undesired fragmentation of abatacept, whereas thrombin did not cleave the molecule with any significant yield, in spite of previous reports

Table 1: Parameters for Chaotrope-Induced and Thermally Induced Unfolding at pH 6 and 7.5 Monitored by Intrinsic Fluorescence

		pH 6	pH 7.5
GdnHCl, 25 °C	ΔG_1, kJ/mol	7.1 ± 0.6	15.6 ± 1.2
	ΔG_2, kJ/mol	33.1 ± 1.8	44.3 ± 0.9
	C_{m1}, mol/L	0.8 ± 0.1	1.3 ± 0.2
	C_{m2}, mol/L	2.9 ± 0.2	3.6 ± 0.1
urea, 25 °C	ΔG_1, kJ/mol	6.8 ± 1.3	14.5 ± 1.3
	ΔG_2, kJ/mol	47.3 ± 3.9	nd[a]
	C_{m1}, mol/L	3.1 ± 0.2	3.8 ± 0.2
	C_{m2}, mol/L	8.6 ± 0.3	nd
temperature	T_{m1}, °C	47.7 ± 0.1	51.6 ± 0.3
	T_{m2}, °C	80.9 ± 0.2	78.5 ± 0.2

[a]nd = not determined due to short baseline.

that thrombin exhibits proteolytic activity against the EPK sequence found in the hinge region of abatacept that links the two domains (*45*, *46*).

In another approach, we used CTLA-4 that was produced in *E. coli* to measure the T_m for thermal unfolding of CTLA-4. The observed T_m, 58 °C at pH 7.5 (far-UV CD), was close to that of the first thermal transition observed for abatacept. Because CTLA-4 produced in *E. coli* is not glycosylated, we also measured the T_m's for unfolding of abatacept after treating the protein with PNGase F to deglycosylate the molecule. Deglycosylation resulted in only minor decreases (ca. 2.5 and 1 °C for the first and second transition, respectively) in the observed T_m values. Depending on solution conditions and heating rates, T_m values for Fc domains in intact antibodies are generally in the range of 80−84 °C, with the C_H3 domain generally more stable than the C_H2 domain (*24*, *25*, *47*), which corresponds well to the second transition in abatacept (83 °C at a scan rate of 60 °C/h).

DSC scans to 60 °C (a temperature between the first and second transitions), followed by cooling and reheating to 60 °C, show 50% recovery of peak area measured in the first scan. Further scans on the same sample result in close to 100% recovery of the peak area seen in the second scan (Figure 8B). This indicates that the low-temperature transition is a composite of one irreversible and one highly reversible population with equal changes in heat capacity upon unfolding. In an earlier study (*48*), a DSC thermogram of a Fc domain with a sequence similar to that in abatacept shows a T_m for the C_H2 domain of ca. 60 °C, close to the first transition measured in our study. These results imply that the thermal unfolding transitions of the CTLA-4 and the C_H2 domains likely overlap to give the first observed transition, whereas unfolding of the C_H3 domain is responsible for the second transition. Therefore, we assign the lower temperature transition to the CTLA-4 and C_H2 domains and the high-temperature transition to the C_H3 domain of abatacept.

Chaotrope-Induced Unfolding of Abatacept. Fluorescence Spectroscopic Analysis of the Fc Domain. GdnHCl- and urea-induced denaturation monitored by intrinsic fluorescence of tryptophan residues in the Fc domain of abatacept at 25 °C yields two transitions at pH 6 and 7.5 (Figure 6A and 6A insert). The first transition is assigned to overlapping CTLA-4 and C_H2 domain unfolding, and the second transition is assigned to C_H3 domain unfolding (for more details see the Discussion).

Fitting a two-state model to each transition in GdnHCl (Figure 6A) yields the unfolding free energy and a midpoint of transition (C_m) for the first and second transition that is shown in Table 1. For the first transition the m values are -9.0 ± 0.6 and

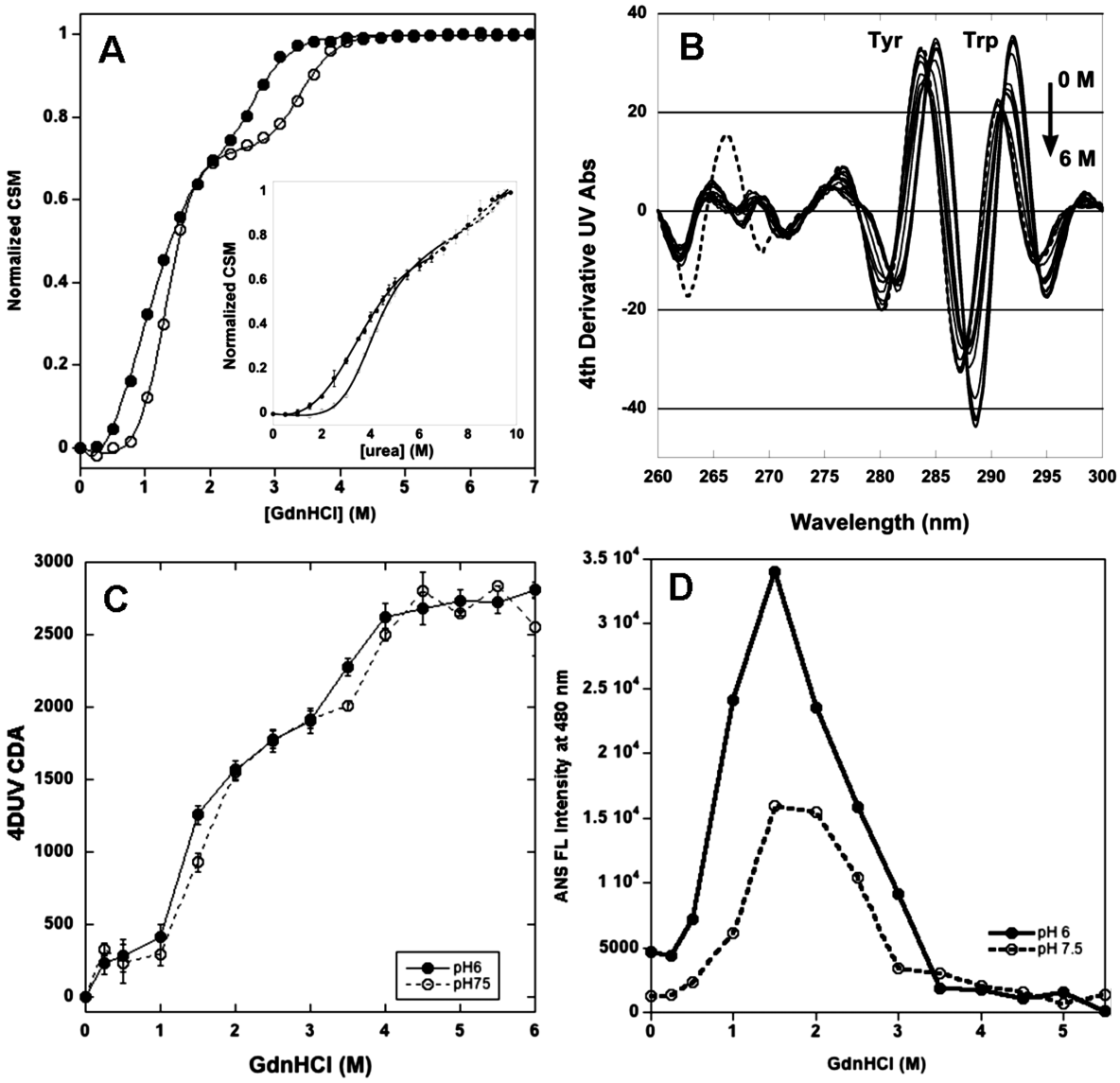

FIGURE 6: (A) GdnHCl denaturation of abatacept at pH 6 (filled circles) and pH 7.5 (open circles) monitored by fluorescence CSM. Insert: Denaturation curves in 0−9.75 M urea of abatacept at pH 6 (filled circles) and pH 7.5 (open circles). (B) 4DUV scans at pH 6 between 260 and 310 nm of abatacept in 0−6 M GndHCl. (C) Denaturation curve in 0−6 M GdnHCl of abatacept at pH 6 (filled circles) and pH 7.5 (open circles) plotted as CDA from 4DUV. (D) ANS fluorescence in the presence of abatacept (ca 100:1 molar ratio) at pH 6 (filled circles) and pH 7.5 (open circles) in 0−5.5 M GdnHCl. Samples in all figures are all in 10 mM sodium phosphate with 25 mM NaCl and monitored at 25 °C.

-12.1 ± 1.0 kJ/mol at pH 6 and 7.5, respectively. The second transitions have *m* values of -11.6 ± 0.5 and -12.4 ± 0.2 kJ/mol at pH 6 and 7.5, respectively.

Urea solutions at 25 °C for abatacept also yield two unfolding transitions at pH 6 and 7.5 (Figure 6A insert). Fitting a two-state model to each transition yields free energy of unfolding and C_m that are shown in Table 1. Abatacept is more stable toward urea than GdnHCl. Unfolding *m* values for the first transition at pH 6 and 7.5 are -2.2 ± 0.4 and -3.7 ± 0.4 kJ/mol, respectively. The second transition yields an *m* value of -5.5 ± 0.4 kJ/mol at pH 6, but at pH 7.5 this transition cannot be reliably analyzed because unfolding is not complete even in saturated urea solutions.

The CSM values for the native and unfolded state of abatacept in both GdnHCl and urea solutions are independent of pH and are located at 338 and 351 nm, respectively. The CSM for free trypthophan is typically around 350 nm; thus it appears that the aromatic residues of abatacept are fully solvent exposed in the final state. An intermediate state with a CSM around 346 nm is evident at GdnHCl concentrations around 2 M, and similarly at urea concentrations of 5.5 M.

Reversibility studies of the GdnHCl-induced unfolding transitions show a two-state transition with a C_m of ca. 2 M for the refolding, a value in between the two unfolding transitions (Supporting Information Figure 2). The CSM observed after dilution from 7 M GdnHCl to 0.25 M GdnHCl is 340 nm, compared to 338 nm observed at the same GdnHCl concentrations during unfolding. The change in apparent number of folding steps and shift in CSM during refolding compared to unfolding experiments indicates partial reversibility of the unfolding transition.

4DUV Spectroscopy. A blue shift and decreased intensity in the 4DUV spectral signal is observed for the peaks arising from tryptophan residues during GdnHCl denaturation (Figure 6B), whereas peaks arising from tyrosine first decrease in intensity and then increase. GdnHCl also causes a blue shift of the peaks from tyrosine absorbance. Blue shifts suggest an increase in the polarity of the aromatic environment as the protein unfolds.

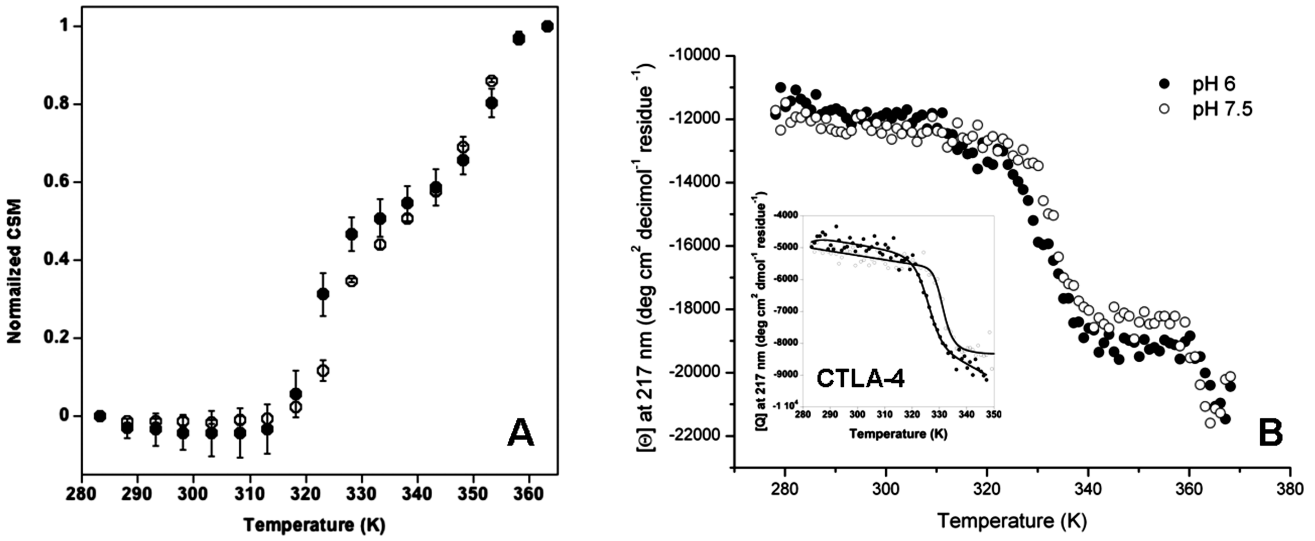

FIGURE 7: (A) Fluoresence CSM of thermal denaturation of abatacept at pH 6 (filled circles) and pH 7.5 (open circles) between 10 and 95 °C. (B) Far-UV CD melt followed between 10 and 95 °C at 217 nm for abatacept and CTLA-4 (insert) at pH 6 (filled circles). All samples and pH 7.5 (open circles). All samples in 10 mM sodium phosphate buffer and 25 mM NaCl.

As tyrosine residues are fairly evenly distributed in abatacept, the tyrosine-optimized derivative analysis likely reflects the "global" unfolding of the protein. The spectral changes in the fourth derivative data were expressed as the cumulative difference amplitude (CDA) (*34*). Figure 6C shows a three-state transition at both pH 6 and pH 7.5. The GdnHCl concentrations at the midpoints of the first and second transitions observed at pH 6 are 1.3 and 3.5 M, respectively, and 1.4 and 3.9 M, respectively, at pH 7.5.

ANS Fluorescence. ANS fluorescence was followed to probe changes in exposure of hydrophobic regions upon denaturation, but charge interactions can modify the fluorescence/binding behavior of ANS (*49*, *50*). In GdnHCl at 25 °C, ANS interacts significantly with abatacept between 0.5 and 3 M GdnHCl; this region correlates with the first transition and the intermediate area. The ANS fluoresence intensity is more pronounced at pH 6 compared to pH 7.5, with almost a 2-fold higher maxiumum intensity at 480 nm and a slightly wider fluorescence range (Figure 6D).

Thermally Induced Unfolding of Abatacept. The thermal stability of abatacept in solution was determined using DSC, far-UV CD, and intrinsic fluoresence at pH 6 and 7.5. Fluorescence (Figure 7A) and CD (Figure 7B) show two distinct transitions upon heating. DSC exhibits two main transitions around 50 and 80 °C, with additional transitions detectable at higher temperatures (T > 90 °C) that probably are aggregation-related. All transitions are scan rate and pH dependent (Figure 8A and Table 2). Thermal denaturation is essentially 100% irreversible (Supporting Information Figure 3).

Fluorescence Spectroscopic Monitoring of Thermally Induced Unfolding in the Fc Domain of Abatacept. Thermally induced unfolding of abatacept monitored from 10 to 90 °C in sodium phosphate buffer exhibits two transitions in solutions at both pH 6 and pH 7.5 (Figure 7A). The transitions observed are likely unfolding of the C_H2 and C_H3 domains as CTLA-4 does not contain any Trp. Fitting a two-state model to each transition individually yields transition midpoint temperatures (T_m) that are shown in Table 1. The CSM for the unfolded state (90 °C) is around 346 and 348 nm for solutions at pH 6.0 and 7.5, respectively. An intermediate state observed at 62 °C has a CSM around 343.5 nm. It should be noted that both the unfolded and intermediate states observed at elevated temperatures have

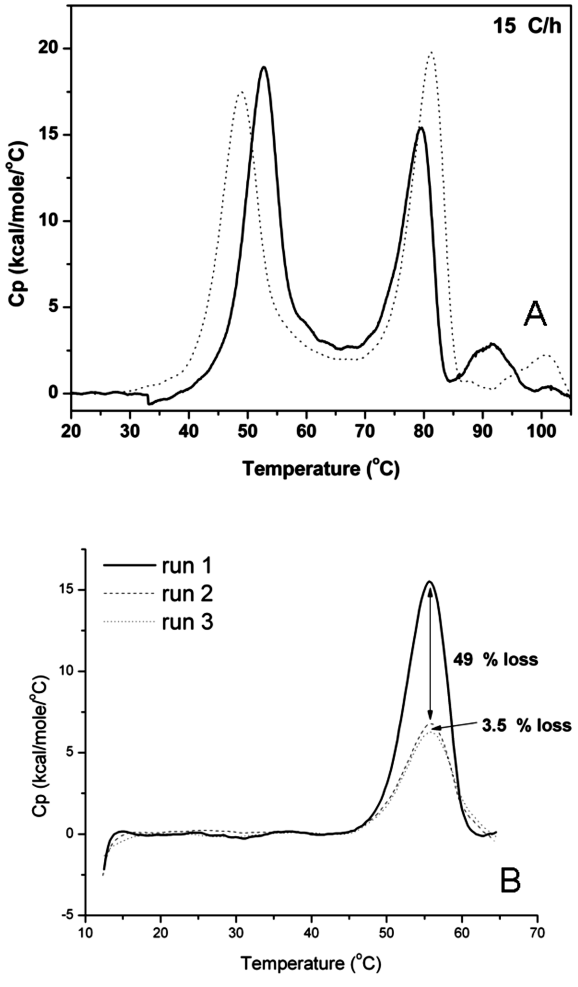

FIGURE 8: (A) DSC thermograms between 20 and 105 °C of abatacept in sodium phosphate buffer at pH 6 (dotted) and pH 7.5 (solid). (B) Refolding of first thermal transition between 15 and 65 °C of abatacept in 10 mM sodium phosphate and 25 mM NaCl at pH 7.5. First heat−cool−heat cycle yields 51% reversibility (solid to dashed), and second cycle yields 96.5% reversibility (dashed to dotted).

Table 2: DSC Transition Midpoint Temperatures at Different Scan Rates and Transition Activation Energies at pH 6 and 7.5[a]

	pH 6			pH 7.5		
scan rate (°C/h)	T_{m1} (°C)	T_{m2} (°C)	T_{m3} (°C)	T_{m1} (°C)	T_{m2} (°C)	T_{m3} (°C)
15	48.8	81.2	100.2	52.7	79.6	91.6
30	50.5	82.2	100.5	54.2	81.1	93.8
60	52.6	84.9		55.8	83.0	95.5
90	54	85.9		57.1	84.3	
E_a,[c] kJ/mol	297 ± 13	391 ± 14	−[b]	361 ± 19	391 ± 20	422 ± 18

[a] $dH < dH_v$ for transition 3 → aggregation. Aggregation kinetics faster at pH 6 than pH 7.5 as T_m is less scan rate dependent at pH 6 compared to pH 7.5 (see Supporting Information Table 2). [b] A third transition is not detected at the higher scan rates at pH 6, precluding estimation of the activation energy. [c] Standard errors from fitting.

different CSM values compared to those measured in urea or GdnHCl solutions, indicating less solvent exposure of aromatics at elevated temperature than in chaotrope solutions.

Far-UV CD Monitoring of Thermally Induced Unfolding in Abatacept. Thermally induced unfolding followed by far-UV CD at 217 nm at temperatures from 10 to 95 °C in sodium phosphate buffer yields two transitions at both pH 6 and pH 7.5 (Figure 7B), with a decreasing CD signal with increasing temperature, typical for β-sheet proteins. We expect to observe the unfolding of all domains as far-UV CD monitors the protein backbone. As we only can observe two transitions, CTLA-4 unfolding is overlapping with the C_H2 domain unfolding in the first transition (see Discussion). CD measurements coupled with heat capacity values determined from DSC experiments were used to yield T_m values for the first transition of 59.5 ± 0.7 °C at pH 6 and 60.4 ± 0.4 °C at pH 7.5. The second transition has a T_m = 89.4 ± 4.6 °C for pH 6 and 87.7 ± 2.4 °C at pH 7.5. The posttransitional baseline is short and noisy due to the proximity to the lower boiling point due to altitude (ca. 94−95 °C at 1600 m above sea level).

Differential Scanning Calorimetric Analysis of Abatacept Unfolding. Thermally induced unfolding monitored by calorimetry shows two major transitions and additional scan rate- and pH-dependent transitions (Figure 8A). T_m values at different scan rates are tabulated in Table 2. As observed in fluorescence and CD studies, the second transition has higher thermal stability at pH 6 compared to that at pH 7.5. In contrast, the first transition is more stable at pH 7.5. The T_m's are intermediate between those obtained by fluorescence and CD. Unfolding is irreversible after full unfolding, but if heating is stopped after the first transition (ca. 60 °C) and the sample is cooled to 10 °C, a subsequent heating to 60 °C shows a 50% recovery of the excess heat capacity observed during the first run, indicating partial reversibility. Interestingly, a third scan gives 96.5% reversibility relative to the second scan (Figure 8B). The T_m's were not affected by varying abatacept concentrations from 1 to 11 mg/mL at either pH (Supporting Information Figure 4). Lower van't Hoff enthalpies compared to the calorimetric enthalpies in the two first transitions for all scan rates indicate that those transitions are not two-state unfolding reactions. For the third transition, the van't Hoff enthalpies are higher compared to the calorimetric enthalpies, consistent with aggregation reactions being responsible for the observed excess heat capacity (Supporting Information Table 1).

Table 3: Second Virial Coefficient (SVC) from Light Scattering and Zeta Potential from Laser Doppler Velocimetry for Abatacept at pH 6 and 7.5 in 10 mM Sodium Phosphate and 25 mM NaCl (Ionic Strength = 75 mM) at 25 °C

	light scattering		laser Doppler velocimetry		
pH	SVC × 10^{-4} (mL mol g^{-2})	M_w × 10^3 (g mol^{-1})	zeta potential (mV)	SVC_{el} × 10^{-6} (mL mol g^{-2}) (% of SVC)	effective charge (Z)/ theoretical charge
6	−6.5 ± 3.7	78.9 ± 2.7	−9.3 ± 1	2.8 (0.4%)	−2.6/−2
7.5	−6.0 ± 1.9	68.6 ± 3.0	−12.8 ± 1.2	5.2 (0.9%)	−3.5/−14.8

Heat Capacity Changes during Thermally Induced Unfolding of Abatacept. At pH 6, complete abatacept unfolding, CTLA-4/C_H2 domain unfolding, and C_H3 domain unfolding yielded heat capacity changes of 5.2, 3.1, and 2.1 kcal mol^{-1} K^{-1}, respectively. At pH 7.5 those heat capacity changes were 8.0, 5.7, and 2.3 kcal mol^{-1} K^{-1}, respectively (Supporting Information Figure 3). The heat capacity change for unfolding of abatacept was estimated to 8.4 kcal mol^{-1} K^{-1} based on the primary sequence (*51*), close to the experimental value at pH 7.5.

Scan Rate Dependence and Activation Energies. T_m values increase with increasing scan rates (Table 2). The activation energies for each transition are tabulated in Table 2. Activation energies were pH dependent for the lower temperature transition. At both pHs, activation energies were smaller for the lower temperature transition.

Thermally Induced Unfolding in Deglycosylated Abatacept and CTLA-4. Thermally induced unfolding of abatacept deglycosylated with PNGase F and *E. coli*-expressed CTLA-4 (thus aglycosylated) was followed by DSC, far-UV CD, or intrinsic fluorescence. For deglycosylated abatacept in pH 7.5 sodium phosphate buffer, the first transition midpoint temperature is lowered by around 2 °C compared to that in complete abatacept, whereas the second transition midpoint temperature is affected by less than 1 °C compared to the abatacept (Supporting Information Figures 5 and 6). The denaturation is irreversible, and the solution is opaque afterward, indicating the presence of insoluble aggregates.

The thermal stability of the CTLA-4 covalent dimer in sodium phosphate buffer was monitored using DSC and far-UV CD. Melting followed by far-UV CD at 217 nm shows one single transition with midpoint transition temperatures of 52.3 and 58.4 °C at pH 6 and 7.5, respectively (Figure 7B insert). A single transition with a T_m of 54.4 °C is also seen using DSC at pH 8 in 20 mM Tris, 200 mM NaCl, and 10% glycerol (Supporting Information Figure 7). The thermal denaturation is irreversible.

Colloidal Stability. Zeta Potentials and Second Osmotic Virial Coefficient from Light Scattering (SVC). The SVC are negative at both pH 6 and pH 7.5, indicating net pairwise attraction between abatacept molecules (Table 3). By measuring the zeta potential from the electrophoretic mobility of abatacept, the electrostatic contribution to its solution behavior could be measured at pH 6 and 7.5. As seen in Table 3, pH 6 solution conditions show slightly lower negative zeta potential compared to pH 7.5 conditions. Both values are well below the arbitrary limit for colloidal stability of ±30 mV (*52*). The Debye−Huckel approximation (eq 10) yields estimated effective charges at both pH conditions that are negative and only separated by one charge unit. At pH 6, the theoretical and the

effective charges are very close, but the effective charge at pH 7.5 is ca. 4-fold less negative than the theoretical charge. This effective charge measured at the diffuse layer boundary or slipping plane contributes to the intermolecular interactions and is reflected in the estimate of the electrostatic contribution to the SVC (Table 3). At both pH 6 and pH 7.5 this contribution is insignificant, and the net attractive SVC in sodium phosphate buffer can be explained by both the low protein surface charge and electrostatic screening of the remaining charges.

DISCUSSION

Aggregation Profile of Abatacept/Lumry−Eyring Framework. During incubation studies at 40 °C, abatacept aggregated much more rapidly in solutions at pH 6.0 than at pH 7.5. Based on the Lumry−Eyring theory (*10*), we expect that the increased aggregation rate seen at pH 6.0 vs pH 7.5 could be due to decreased conformational stability of abatacept at the lower pH or more attractive intermolecular interactions (decreased colloidal stability) or both.

Aggregation generally does not require complete unfolding but rather proceeds via partially unfolded intermediates (*6*, *8*). In support of this expectation, we observed that abatacept is susceptible to aggregation at moderately elevated temperature (40 °C), even though complete unfolding of the molecule requires relatively high concentrations of chaotrope (> 9 M urea), and elevated temperatures (> 90 °C). At temperatures from 10 to 40 °C, no differences in abatacept structure can be detected in solutions at pH 6.0 vs pH 7.5 using far-UV CD or second derivative UV absorbance spectroscopy, suggesting that the majority of the protein remains in the native state ensemble under both pH conditions.

Molten Globule-like Intermediate in the Lumry−Eyring Scheme. If a molten globule intermediate is formed as a protein unfolds, techniques that monitor secondary vs tertiary structural changes often show different onset points for the unfolding transition, with tertiary structure losses preceding disappearance of secondary structures (*53*, *54*). Under identical solution conditions, the apparent midpoints for thermally induced unfolding transitions of abatacept detected using various spectroscopic techniques increase in the order fluorescence < DSC < far-UV CD (Table 1). This indicates an intermediate state during the melting where the secondary structure, probed by far-UV CD, is more stable than the tertiary structure that is reflected in the tryptophan environment as probed by fluorescence. Calorimetry measurements, which follow overall thermal processes during unfolding, show transition temperatures in between those detected by fluorescence or far-UV CD.

ANS fluorescence as a function of GdnHCl is consistent with formation of an intermediate state with greater exposed hydrophobic surface area that is populated at moderate GdnHCl concentrations (e.g., 0.5−3.5 M). ANS fluorescence is more pronounced at pH 6, suggesting that the intermediate state has increased solvent-accessible hydrophobic regions at pH 6 than at pH 7.5.

A likely model for an aggregation-prone abatacept intermediate is a hybrid of molten globule-like CTLA-4 and C_H2 domains and an intact C_H3 domain. If a partially unfolded state is involved in the aggregation reaction, we expect that the stability of the least stable domain will dominate the conformational stability contributions to aggregation (*13*, *15*). In the case of abatacept, the CTLA-4 and C_H2 domains are less stable than the C_H3 domain at both solution conditions tested. Using chaotropes to perturb the structure of abatacept, we found that the free energy of unfolding of the CTLA-4/C_H2 domains decreases by approximately a factor of 2 (15.6−7.1 kJ/mol) as the pH decreases from 7.5 to 6.0. Thus, a contributing factor to increased aggregation rates at pH 6 may be the greater instability of the CTLA-4/C_H2. In contrast, the stability of the C_H3 domain decreases by 25% (44.3 to 33.1 kJ/mol) upon decreasing pH from 7.5 to 6.0 and is always significantly higher than that of the CTLA-4/C_H2.

In addition, the apparent activation energy for domain unfolding is pH dependent for the CTLA-4/C_H2 domains but not for the C_H3 domain (Table 2), suggesting that the pH sensitivity in rates of aggregation is related to pH-induced changes in the stability of the CTLA-4/C_H2 domains rather than in the C_H3 region. Furthermore, the theoretical heat capacity change of unfolding per residue for CTLA-4/C_H2 domains is larger than that for the C_H3 domain, suggesting that unfolding increases solvent exposure of hydrophobic residues to a greater degree for CTLA-4 compared to the Fc domain of abatacept (*55*). Thus, unfolded or partly folded CTLA-4/C_H2 domains would be expected to be more prone to aggregation via hydrophobic interactions than the C_H3 domain. All of those contributions would result in a larger fraction of partly unfolded aggregation-prone species at pH 6 compared to pH 7.5 at 40 °C.

Colloidal Stability. The second step in the general Lumry−Eyring framework is a collisional reaction step, which is expected to be influenced by the intermolecular forces between abatacept molecules. Typically, these forces are dominated by electrostatic interactions (*56*). Overall, the measured p*I* for abatacept is 4.5−5.5, based on isoeletric focusing. Thus, we would expect that the intermolecular electrostatic interactions would be repulsive, since abatacept should carry a negative charge at both pH 6.0 and pH 7.5. Indeed, this is borne out by the zeta potential values for abatacept (−9.3 and −12.8 mV at pH 6.0 and 7.5, respectively). However, for colloidal stability, the absolute value of the zeta potential should be greater than 30 mV (*52*, *56*), an empirical value that separates low-charged surfaces from high-charged surfaces, so abatacept appears to be colloidally unstable at both solution pHs but only slightly more so at pH 6.

Interestingly, the p*I*'s of the individual domains (calculated based on amino acid sequence, but not taking potential counterion binding into account) are near 7.2 and 4.2 for the Fc and CTLA-4 domains, respectively, compared to the calculated p*I* of 5.9 for the whole molecule. The calculated p*I*'s are 8.9 and 6.5 for the C_H2 and C_H3 Fc subdomains, respectively. Thus, whereas at pH 7.5 the charge calculated based on amino acid sequence on both domains will be negative (−14.2 for CTLA-4, −0.6 for Fc, but +2.3 for C_H2, and −3 for C_H3), at pH 6.0 the CTLA-4 domain is expected to be negatively charged (−12) and the Fc domain positively charged (+10), with +8 for C_H2 and +2.2 for C_H3 (Supporting Information). These opposite charges would be expected to increase domain−domain intramolecular attractive interactions at pH 6.0 and also to increase intermolecular attraction via increased dipole−dipole interactions. The observation of pH-dependent dimer and trimer populations as a result of accelerated stability studies may originate from the different domain charge distributions at the two pH conditions.

The SVC values for abatacept do not differ significantly at the two pH values studied, consistent with the measured zeta potentials. Although the SVC values under both conditions are negative, reflecting attractive protein−protein pairwise

interactions, the similarity of the SVC values suggests that differences in colloidal instabilities at pH 6.0 and 7.5 are not responsible for the large differences in rates of aggregation at the two pHs. This conclusion is further substantiated by the fact that at room temperature, well below temperatures where the thermal transitions are observed, abatacept does not aggregate appreciably over at least 30 days when stored at either pH. Rapid aggregation did not allow SVC determination at elevated temperatures.

Based on the calculated charge distribution on abatacept at pH 6.0, strong electrostatic contributions to the SVC might be expected. However, based on zeta potential measurements made in solution, the electrostatic contribution to the SVC is insignificant. This may arise from both counterion binding that reduces the effective surface charges of abatacept at the two pH conditions and from electrostatic screening of remaining charges at the ionic strength tested (75 mM). The relatively small net attractive pairwise interactions may be explained by van der Waals attractions and/or by attractive dipolar interactions because of the opposite charges of various domains. Interestingly, the SVC in pH 6 and 7.5 solutions containing 50 mM Tris, 25 mM MES, 25 mM acetic acid, and 25 mM NaCl (a solution with the same, but pH-independent, ionic strength of 75 mM), instead of phosphate, is positive at both pH conditions, implying repulsive net pairwise interactions. This could indicate that binding of phosphate ions to abatacept has an important role in making abatacept self-interactions attractive but is beyond the scope of the current study.

CONCLUSION

At 40 °C, abatacept shows strikingly different propensity to aggregate at pH 6.0 compared to pH 7.5. This propensity correlates with the pH effect on conformational stability of the domains of abatacept. In contrast, colloidal stability of abatacept is relatively insensitive to the pHs studied. This suggests that partial unfolding of the least stable domains dominates abatacept's aggregation propensity.

Because protein aggregation generally proceeds through partially unfolded intermediates, it is likely that the least stable domain of a multidomain protein will predominately determine the aggregation propensity of the protein. In the case of abatacept, the CTLA-4/C_H2 domains appear to be much less stable than the more stable C_H3 domain and thus likely are responsible for abatacept aggregation under accelerated aggregation conditions.

Intact antibodies have generally a good temperature tolerence, as exemplified by the lack of any negative effect on the biological activity after the use of heat treatment at 60 °C for 10 h (pasteurization) of intravenous Ig preparations for viral clearance (*57*). In comparison with native IgG proteins, wherein interdomain interactions presumably have evolved to provide mutual stabilization, fusion proteins may lack such stabilizing interdomain stabilization. This is the case for abatacept: the unfolding transitions show minimal cooperativity between domains. This has been seen in other artificial fusion proteins as well (*58*). In contrast, many natural multidomain proteins such as antibodies show cooperative transitions that are apparent two state (*21*).

As with most randomly introduced mutations, fusion of two or more foreign proteins or domains would be expected only rarely to create stabilizing, cooperative interactions. There may be a vast potential to increase the stability and modulate aggregation properties of artificial fusion proteins by optimizing inter- and intramolecular domain−domain interactions by not only adjusting formulation conditions but using protein engineering approaches.

ACKNOWLEDGMENT

LaToya Jones Braun's laboratory at the School of Pharmacy and the Biophysical Core Center at the University of Colorado in Denver are acknowledged for instrument access. Ingemar Andre at David Baker's laboratory at the University of Washington, Seattle, is gratefully thanked for helpful discussions concerning structural modeling with Robetta and PyMOL. Barofold is gratefully thanked for donating CTLA-4. Malvern Inc. is acknowledged for help with zeta potential and DLS measurements. Joan Torrent and Reinhard Lange, INSERM, Montpellier, France, are gratefully thanked for providing software for CDA calculations, as well as for helpful comments on the manuscript.

SUPPORTING INFORMATION AVAILABLE

Further calorimetric, AUC, charge distribution calculations, deglycosylation stability, and reversibility data for abatacept and CTLA-4. This material is available free of charge via the Internet at http://pubs.acs.org.

REFERENCES

1. Uversky, V., and Fink, A., Eds. (2006) Protein Misfolding, Aggregation and Conformational Diseases, Vol. 1−2, Kluwer Academic/Plenum, New York.
2. Wang, W. (2005) Protein aggregation and its inhibition in biopharmaceutics. *Int. J. Pharm. 289*, 1–30.
3. Rosenberg, A. (2006) Effects of protein aggregates: An immunologic perspective. *AAPS J. 8*, 501–507.
4. Regina, M., and Murphy, B. S. K. (2007) Protein misfolding and aggregation. *Biotechnol. Prog. 23*, 548–552.
5. Cromwell, M., Hilario, E., and Jacobson, F. (2006) Protein aggregation and bioprocessing. *AAPS J. 8*, 572–579.
6. Roberts, C. J. (2007) Nonnative protein aggregation kinetics. *Biotechnol. Bioeng. 98*, 927–938.
7. Andrews, J. M., and Roberts, C. J. (2007) A Lumry−Eyring nucleated polymerization model of protein aggregation kinetics: 1. Aggregation with pre-equilibrated unfolding. *J. Phys. Chem. B 111*, 7897–7913.
8. Chi, E. Y., Krishnan, S., Randolph, T. W., and Carpenter, J. F. (2003) Physical stability of proteins in aqueous solution: Mechanism and driving forces in nonnative protein aggregation. *Pharm. Res. 20*, 1325–1336.
9. Mahler, H. C., Friess, W., Grauschopf, U., and Kiese, S. (2008) Protein aggregation: Pathways, induction factors and analysis, J. Pharm. Sci. (published online Sept 29).
10. Lumry, R., and Eyring, H. (1954) Conformation changes of proteins. *J. Phys. Chem. 58*, 110–120.
11. Batey, S., and Clarke, J. (2006) Apparent cooperativity in the folding of multidomain proteins depends on the relative rates of folding of the constituent domains. *Proc. Natl. Acad. Sci. U.S.A. 103*, 18113–18118.
12. Randles, L. G., Batey, S., Steward, A., and Clarke, J. (2008) Distinguishing specific and nonspecific interdomain interactions in multidomain proteins. *Biophys. J. 94*, 622–628.
13. Azuaga, A. I., Dobson, C. M., Mateo, P. L., and Conejero-Lara, F. (2002) Unfolding and aggregation during the thermal denaturation of streptokinase. *Eur. J. Biochem. 269*, 4121–4133.
14. Chi, E. Y., Krishnan, S., Kendrick, B. S., Chang, B. S., Carpenter, J. F., and Randolph, T. W. (2003) Roles of conformational stability and colloidal stability in the aggregation of recombinant human granulocyte colony-stimulating factor. *Protein Sci. 12*, 903–913.
15. Oganesyan, V., Damschroder, M. M., Leach, W., Wu, H., and Dall'Acqua, W. F. (2008) Structural characterization of a mutated, ADCC-enhanced human Fc fragment. *Mol. Immunol. 45*, 1872–1882.
16. Salinas, B. (2009) Phase behaviour and opalescence of concentrated antibody formulations, in Chemical and Biological Engineering, University of Colorado, Boulder, CO.

17. Chou, D. K., Krishnamurthy, R., Randolph, T. W., Carpenter, J. F., and Manning, M. C. (2005) Effects of Tween 20 and Tween 80 on the stability of Albutropin during agitation. *J. Pharm. Sci. 94*, 1368–1381.
18. Chamow, S. M., and Ashkenazi, A., Eds. (1999) Antibody Fusion Proteins, 1st ed., Wiley-Liss, New York.
19. Teillaud, J.-L. (2005) Engineering of monoclonal antibodies and antibody-based fusion proteins: Successes and challenges. *Expert Opin. Biol. Ther. 5*, S15–S27.
20. Wang, W., Singh, S., Zeng, D. L., King, K., and Nema, S. (2007) Antibody structure, instability, and formulation. *J. Pharm. Sci. 96*, 1–26.
21. Honegger, A. (2008) Engineering antibodies for stability and efficient folding, in Therapeutic Antibodies (Chernajovsky, Y., and Nissim, A., Eds.) pp 47−68, SpringerLink.
22. Daugherty, A. L., and Mrsny, R. J. (2006) Formulation and delivery issues for monoclonal antibody therapeutics. *Adv. Drug Delivery Rev. 58*, 686–706.
23. Ionescu, R. M., Vlasak, J., Price, C., and Kirchmeier, M. (2008) Contribution of variable domains to the stability of humanized IgG1 monoclonal antibodies. *J. Pharm. Sci. 97*, 1414–1426.
24. Liu, H., Bulseco, G.-G., and Sun, J. (2006) Effect of posttranslational modifications on the thermal stability of a recombinant monoclonal antibody. *Immunol. Lett. 106*, 144–153.
25. Demarest, S. J., and Glaser, S. M. (2008) Antibody therapeutics, antibody engineering, and the merits of protein stability. *Curr. Opin. Drug Discovery Dev. 11*, 675–687.
26. Garber, E., and Demarest, S. J. (2007) A broad range of Fab stabilities within a host of therapeutic IgGs. *Biochem. Biophys. Res. Commun. 355*, 751–757.
27. Linsley, P., Brady, W., Urnes, M., Grosmaire, L., Damle, N., and Ledbetter, J. (1991) CTLA-4 is a second receptor for the B cell activation antigen B7. *J. Exp. Med. 174*, 561–569.
28. Moreland, L., Bate, G., and Kirkpatrick, P. (2006) Abatacept. *Nat. Rev. Drug Discovery 5*, 185–186.
29. Davis, P. M., Abraham, R., Xu, L., Nadler, S. G., and Suchard, S. J. (2007) Abatacept binds to the Fc receptor CD64 but does not mediate complement-dependent cytotoxicity or antibody-dependent cellular cytotoxicity. *J. Rheumatol. 34*, 2204–2210.
30. Pace, C. N., Vajdos, F., Fee, L., Grimsley, G., and Gray, T. (1995) How to measure and predict the molar absorption coefficient of a protein. *Protein Sci. 4*, 2411–2423.
31. Zhang, Y., Shouvik, R., Jones, L. S., Krishnan, S., Kerwin, B. A., Chang, B. S., Manning, M. C., Randolph, T. W., and Carpenter, J. F. (2004) Mechanism for benzyl alcohol-induced aggregation of recombinant human interleukin-1 receptor antagonist in aqueous solution. *J. Pharm. Sci. 93*, 3076–3089.
32. Krishnan, S., Chi, E. Y., Webb, J. N., Chang, B. S., Shan, D., Goldenberg, M., Manning, M. C., Randolph, T. W., and Carpenter, J. F. (2002) Aggregation of granulocyte colony stimulating factor under physiological conditions: Characterization and thermodynamic inhibition. *Biochemistry 41*, 6422–6431.
33. Lange, R., Frank, J., Saldana, J. L., and Balny, C. (1996) Fourth derivative UV-spectroscopy of proteins under high pressure. 1. Factors affecting the fourth derivative spectrum of the aromatic amino acids. *Eur. Biophys. J. Biophys. Lett. 24*, 277–283.
34. Torrent, J., Connelly, J. P., Coll, M. G., Ribo, M., Lange, R., and Vilanova, M. (1999) Pressure versus heat-induced unfolding of ribonuclease A: The case of hydrophobic interactions within a chain-folding initiation site. *Biochemistry 38*, 15952–15961.
35. Sanchez-Ruiz, J. M. (1992) Theoretical analysis of Lumry−Eyring models in differential scanning calorimetry. *Biophys. J. 61*, 921–935.
36. Pace, C. N. (1986) Determination and analysis of urea and guanidine hydrochloride denaturation curves. *Methods Enzymol. 131*, 266–280.
37. Webb, J. N., Webb, S. D., Cleland, J. L., Carpenter, J. F., and Randolph, T. W. (2001) Partial molar volume, surface area, and hydration changes for equilibrium unfolding and formation of aggregation transition state: High-pressure and cosolute studies on recombinant human IFN-gamma. *Proc. Natl. Acad. Sci. U.S.A. 98*, 7259–7264.
38. Myers, J. K., Pace, C. N., and Scholtz, J. M. (1995) Denaturant m values and heat capacity changes: Relation to changes in accessible surface areas of protein unfolding. *Protein Sci. 4*, 2138–2148.
39. Kratochvil, P. (1987) Classical Light Scattering for Polymer Solutions, Elsevier, Amsterdam, The Netherlands.
40. Arakawa, T., and Wen, J. (2001) Determination of carbohydrate contents from excess light scattering. *Anal. Biochem. 299*, 158–161.
41. Faude, A., Zacher, D., Muller, E., and Bottinger, H. (2007) Fast determination of conditions for maximum dynamic capacity in cation-exchange chromatography of human monoclonal antibodies. *J. Chromatogr. A 1161*, 29–35.
42. Chun, M.-S., and Lee, I. (2008) Rigorous estimation of effective protein charge from experimental electrophoretic mobilities for proteomics analysis using microchip electrophoresis. *Colloids Surf., A 318*, 191–198.
43. Asthagiri, D., Paliwal, A., Abras, D., Lenhoff, A. M., and Paulaitis, M. E. (2005) A consistent experimental and modeling approach to light-scattering studies of protein-protein interactions in solution. *Biophys. J. 88*, 3300–3309.
44. Hsiao, S.-h., and Putnam, F. W. (1961) The cleavage of human ggr-globulin by papain. *J. Biol. Chem. 236*, 122–135.
45. Linsley, P. S., Nadler, S. G., Bajorath, J. R., Peach, R., Leung, H. T., Rogers, J., Bradshaw, J., Stebbins, M., Leytze, G., Brady, W., Malacko, A. R., Marquardt, H., and Shaw, S.-Y. (1995) Binding stoichiometry of the cytotoxic T lymphocyte-associated molecule-4 (CTLA-4). *J. Biol. Chem. 270*, 15417–15424.
46. Muszbek, L., and Laki, K. (1974) Cleavage of actin by thrombin. *Proc. Natl. Acad. Sci. U.S.A. 71*, 2208–2211.
47. Ghirlando, R., Lund, J., Goodall, M., and Jefferis, R. (1999) Glycosylation of human IgG-Fc: Influences on structure revealed by differential scanning micro-calorimetry. *Immunol. Lett. 68*, 47–52.
48. Liu, D., Ren, D., Huang, H., Dankberg, J., Rosenfeld, R., Cocco, M. J., Li, L., Brems, D. N., and Remmele, R. L. (2008) Structure and stability changes of human IgG1 Fc as a consequence of methionine oxidation. *Biochemistry 47*, 5088–5100.
49. Matulis, D., and Lovrien, R. (1998) 1-Anilino-8-naphthalene sulfonate anion-protein binding depends primarily on ion pair formation. *Biophys. J. 74*, 422–429.
50. Gasymov, O. K., and Glasgow, B. J. (2007) ANS fluorescence: Potential to augment the identification of the external binding sites of proteins. *Biochim. Biophys. Acta 1774*, 403–411.
51. Edelhoch, H., and Osborne, J. J. (1976) The thermodynamic basis of the stability of proteins, nucleic acids, and membranes. *Adv. Protein Chem. 30*, 183–250.
52. ASTM Standard (1985) D 4187-82 Test Methods for Zeta Potential of Colloids in Water and Waste Water.
53. Ohgushi, M., and Wada, A. (1984) Liquid-like state of side chains at the intermediate stage of protein denaturation. *Adv. Biophys. 18*, 75–90.
54. Ptitsyn, O. (1995) Molten globule and protein folding. *Adv. Protein Chem. 47*, 83–229.
55. Sturtevant, J. M. (1977) Heat capacity and entropy changes in processes involving proteins. *Proc. Natl. Acad. Sci. U.S.A. 74*, 2236–2240.
56. Everett, D. H. (1988) Basic Principles of Colloid Science, Royal Society of Chemistry, Cambridge, U.K.
57. Bridonneau, P., Marcilly, H., Vernois-Martin, M., Goigoux, P., Bourdel, V., Laulan, A., Deramoudt, F. X., Desmadril, M., Sitbon, M., Basuyaux, B., Steinbuch, M., and Schmitthaeusler, R. (1996) Liquid pasteurization of an immunoglobulin preparation without stabilizer: Effects on its biological and biochemical properties. *Vox Sang. 70*, 203–209.
58. Souillac, P. O. (2005) Biophysical characterization of insoluble aggregates of a multi-domain protein: An insight into the role of the various domains. *J. Pharm. Sci. 94*, 2069–2083.